

Christoph Spijker^{1,*}
Werner Pollhammer²
Harald Raupenstrauch¹


CFD-DEM Modeling of Shaft Furnaces Using the Volume Fraction Smoother Approach

Shaft furnaces are widely used in high-temperature processes for granular materials due to their high energy efficiency. The modeling of these furnaces is challenging because of large domains and long process times. Small geometric details like the natural gas burner nozzles demand a fine grid on the computational fluid dynamics (CFD) side, resulting in a grid size smaller than the particle size. Resolving a discrete element particle over several cells is computationally expensive. Interpolation methods on non-structured grids are complex. In order to provide a fast and simple solution, the volume fraction smoother was developed, and to shorten the calculation time, the time scale splitting method, which separates the time steps for CFD and the discrete-element method (DEM), was introduced.

Keywords: Computational fluid dynamics, Discrete-element method, Shaft furnace, Time scale splitting method, Volume fraction smoother

Received: December 22, 2022; *revised:* February 13, 2023; *accepted:* April 17, 2023

DOI: 10.1002/ceat.202200617

 This is an open access article under the terms of the Creative Commons Attribution License, which permits use, distribution and reproduction in any medium, provided the original work is properly cited.

1 Introduction

Shaft furnaces use off-gas to preheat the granular material in the top part of the furnace and use the hot product after the burning zone to preheat the combustion air. This direct heat exchange leads to high energy efficiency and is widely used in high-temperature processing of granular materials. Due to the constantly moving granular material, measurements inside shaft furnaces are difficult and often the temperature profile, one of the key parameters for energy efficiency of these furnaces, is unknown in industrial processes.

To model the temperature profile of shaft furnaces, the movement of the granular phase in combination with combustion, flow, and heat transfer by conduction, convection, and radiation needs to be considered. The combustion process and the geometry of the gas burner nozzles need an according computational fluid dynamics (CFD) mesh resolution, which is often smaller than the particles. To avoid the computing-intensive process to resolve the discrete-element method (DEM) particles over several CFD cells, the volume fraction smoother (VFS) was created by Pollhammer [1]. This approach enables an accurate representation of the void fraction in the CFD grid in case of larger particles than cells. To further reduce the transient calculation time of the furnace, the time scale splitting method (TSSM) was introduced [1]. This method corrects fluxes to different time scales for heating up the particles.

2 Model Description

2.1 Granular Phase

2.1.1 Particle Flow

For the particle movement and collisions, the basicKinematic-CollidingCloud implemented in OpenFOAM 2.4.0 [2] was used. This model calculates the particle contact forces with the PairSpringSliderDashpot model by Cundall and Strack [3]. To increase the collision time step, the Young's modulus of the particles was decreased from 2.00×10^{11} to 3.77×10^8 Pa, so that the particles at the bottom of the furnace overlap by 2%. Höhner et al. [4] showed that an overlap of 2% has no significant impact on the granular flow. The fluid forces on the particles were modeled by the ErgunWenYuDrag model implemented in OpenFOAM [2].

2.1.2 Particle Thermal Model

The maximum Biot number in the shaft furnace is 0.3. Therefore the assumption of a mean temperature for each particle T_p

¹Dipl.-Ing. Dr.-mont. Christoph Spijker (christoph.spijker@unileoben.ac.at), Univ.-Prof. Dipl.-Ing. Dr. techn. Harald Raupenstrauch Montanuniversitaet Leoben, Chair of Thermal Processing Technology, Franz-Josef-Str. 18, 8700 Leoben, Austria.

²Dipl.-Ing. Dipl.-Ing. Dr.-mont. Werner Pollhammer Montanuniversitaet Leoben, Franz-Josef-Str. 18, 8700 Leoben, Austria.

was chosen for numerical efficiency. The energy equation for each particle is given by Eq. (1), where m_p is the mass of the particle and $c_p(T_p)$ is the temperature-dependent heat capacity. $S_{p,p,rad}$ describes the particle-particle heat transfer by radiation, $S_{p,p,kon}$ the particle-particle and $S_{p,w,kon}$ the particle-wall heat transfer by conduction. Particle-wall radiation is considered in the term $S_{p,w,rad}$. The convective heat transfer to the gas phase is given by $S_{p,p,kon,v}$ modeled by the approach of Gunn [5]. This term is linked to S_p in the gas phase equation for the enthalpy (Eq. (11)) by the numbers of particles in a cell and the acceleration factor of the TSSM.

$$\frac{\partial T_p}{\partial t} m_p c_p(T_p) = S_{p,p,kon} + S_{p,w,kon} + S_{p,p,rad} + S_{p,w,rad} + S_{p,p,kon} \quad (1)$$

2.1.2.1 Particle-Particle Heat Conduction

For modeling the conductive heat transfer between individual particles, the thermal resistance between overlapping particles was modeled based on the approach of Zhang et al. [6] (Eq. (2)). Here, R_{th} is the thermal resistance, and $T_{p,i}$ and $T_{p,j}$ are the temperatures of the contacting particles. Because the particles were softened, the contact areas $A_{p,p}$ were calculated by the forces, using the unsoftened Young's modulus. To evaluate the submodel, the heat flux between two steel particles, with a diameter of 19.8 mm and fixed contact forces, was compared to the measurements by Kuwagi et al. [7] (Fig. 1). The given implementation in the model slightly underestimates the heat flux for high contact forces.

$$S_{p,p,kon,i} = -\frac{A_{p,p}}{R_{th}} (T_{p,i} - T_{p,j}) \quad (2)$$

2.1.2.2 Particle-Wall Heat Conduction

The modeling of the particle-wall conduction uses a similar approach as for the particle-particle conduction. Here as well, the approach from Zhang et al. [6] (Eq. (3)) is used. Based on the wall-particle force for using the unsoftened Young's modulus, a contact area $A_{p,w}$ is calculated. With this contact area and the thermal resistance R_{th} , the heat flux can be obtained. Here, $T_{p,i}$ is the temperature of the particle and $T_{w,i}$ is the temperature of the contacting wall face.

$$S_{p,w,kon,i} = -\frac{A_{p,w}}{R_{th}} (T_{p,i} - T_{w,i}) \quad (3)$$

2.1.2.3 Particle-Particle Radiation

The dominating mechanism for particle-particle heat transfer in a shaft furnace is radiation. To model the radiation between particles in a packed bed, shading must be considered. Feng and Han [8] calculated the view factors $F_{p,p}$ between individual particles in a monodispersed packed bed, considering shading effects. These results are implemented by a fitted function in the model. The approach of a monodisperse bed is valid for a refractory shaft furnace, due to its narrow size distribution. The radiative heat flux is calculated by the Stefan-Boltzmann law (Eq. (4)). Here, σ is the Stefan-Boltzmann constant, A_p is the surface area of the particle, and $T_{p,i}$ and $T_{p,j}$ are the temperatures of the contacting particles.

$$S_{p,p,rad,i} = -\sigma F_{p,p} A_p (T_{p,i}^4 - T_{p,j}^4) \quad (4)$$

2.1.2.4 Particle-Wall Radiation

The analytical solution of the view factor $F_{p,w}$ between a plane and a wall is 0.5. For particles that are contacting the wall, the Stefan-Boltzmann law (Eq. (5)) was applied. Here, $T_{p,i}$ is the temperature of the particle, $T_{w,i}$ is the temperature of the contacting wall face, σ is the Stefan-Boltzmann constant, and A_p is

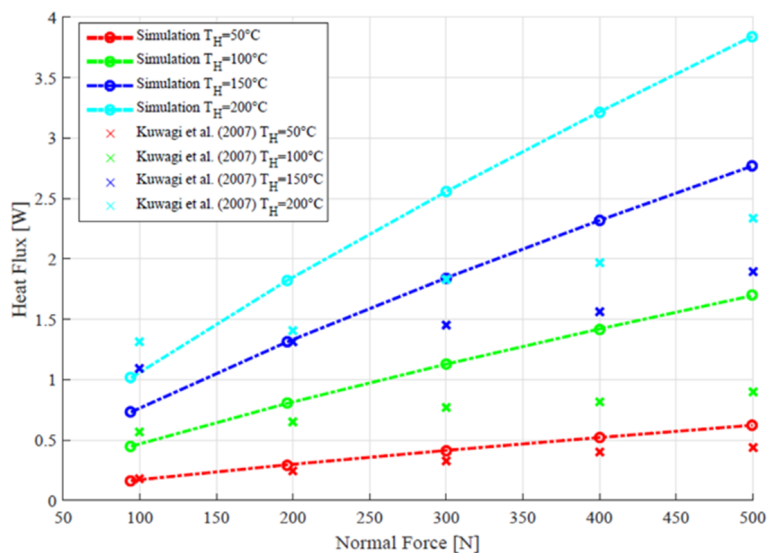


Figure 1. Comparison of the heat flux for different normal forces between the presented model and the measurements of Kuwagi et al. [7] by Pollhammer [1].

the surface area of the particle. If a particle has no wall contact, the particle-wall radiation is neglected.

$$S_{p,w,rad,i} = -\sigma F_{p,w} A_p (T_{p,i}^4 - T_{w,i}^4) \quad (5)$$

2.1.2.5 Evaluation of the Thermal Particle Models

Yagi and Kunii [9] measured the effective heat conductivity of 11-mm iron spheres in a packed bed. This setup was used to evaluate the thermal particle model. The model consists of a packed bed of 11-mm iron spheres between two walls with fixed temperatures (Fig. 2). The hot wall has a temperature of 10 K above the specified temperature and the cold wall is at 10 K below the specified temperature.

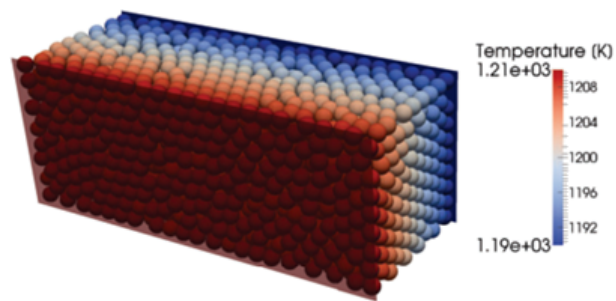


Figure 2. Geometry of the numerical model for evaluating the thermal particle models. The color map shows the temperatures for a reference temperature of 1200 K [1].

Fig. 3 shows the comparison of the model and the experiments of Yagi and Kunii [9], for the effective heat conductivity. The effective heat conductivity is obtained by dividing the heat flux density by the temperature difference of the walls. At lower temperatures, the wall-particle and particle-particle conduction are dominant. With increasing temperatures, radiation gets the dominant form of heat transfer. Inside the range of the measurements from 400 to 1100 K, the model can predict the effective

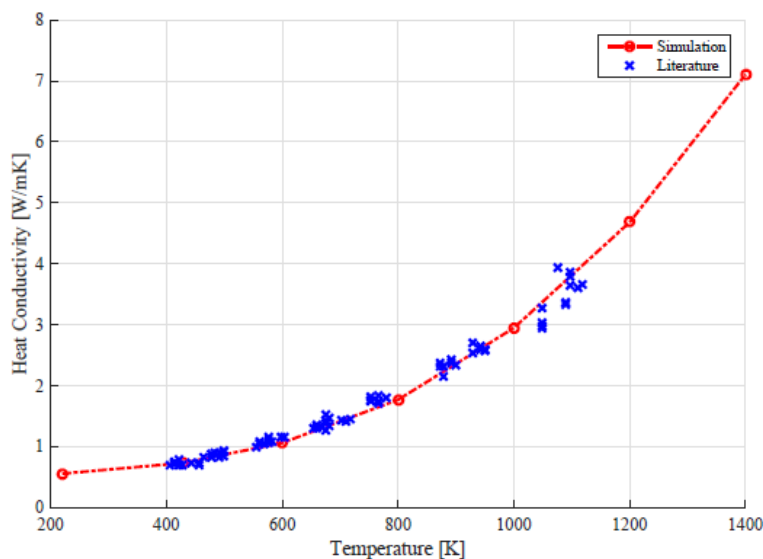


Figure 3. Comparison of the model to the measurements of Yagi and Kunii [9] by Pollhammer [1].

heat conductivity within the range of uncertainty of different measurements.

2.2 Gas Phase

2.2.1 Volume Fraction Smoother

In the presented model, the particles are not resolved in the CFD grid and, in many cases, are larger than the cells. This leads to a particle volume fraction larger than 1 in certain cells (Fig. 4a). Resolving the particle over several CFD cells in each time step, like with the volume penalization method [10], would be too expensive in terms of computing resources. Interpolation methods like the robust hybrid CFD-DEM solver [11] are complex to implement in OpenFOAM [2]. Tests performed with a Gauss equation for the volume fraction show non-physical results. To provide a fast and easy-to-implement algorithm, Pollhammer [1] developed the VFS. The basic idea is to displace the volume fraction in neighboring cells, above a predefined volume fraction threshold ε_{\max} . If, in this step, the neighbor cells reach a volume fraction above the threshold, the smoothing process is continued until all cells have a volume fraction smaller than or equal to the defined threshold ε_{\max} (Fig. 4d). The smoothing algorithm is used at the beginning of each CFD time step.

The operation of the VFS is an iterative process of smoothing steps (Fig. 4). In a smoothing step, first the volume fraction to be transferred to the neighbor cells VF_{tr} is calculated by Eq. (6), where V_{cell} is the volume of the cell, $\varepsilon_{\text{cell}}$ is the initial volume fraction of the cell, and ε_{\max} is the maximal volume fraction of 0.9. Then the cell gets marked as smoothed and the volume fraction of that cell is set to ε_{\max} .

$$VF_{tr} = V_{\text{cell}}(\varepsilon_{\text{cell}} - \varepsilon_{\max}) \quad (6)$$

In the second part of the smoothing step, the transferred volume fraction VF_{tr} is distributed based on the cell volume to the non-smoothed neighbor cells, according to Eq. (7), where

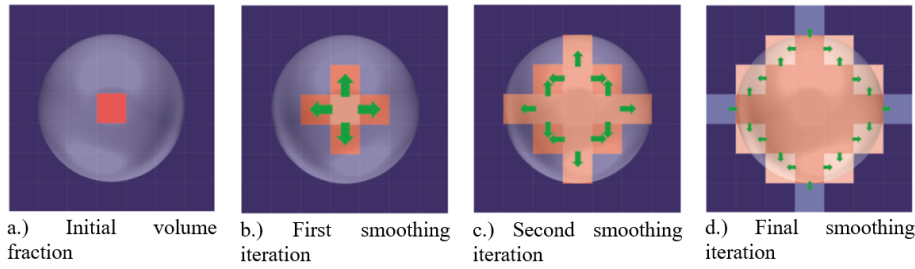


Figure 4. Schematic explanation of the VFS algorithm [1].

$\varepsilon_{\text{neighbor},i,\text{new}}$ is the new and $\varepsilon_{\text{neighbor},i}$ is the current volume fraction of the neighbor cell i . $V_{\text{neighbor},i}$ represents the volume of the neighbor i , and $\sum \varepsilon_{\text{neighbor},j}$ is the volume of all non-smoothed neighbor cells.^{*j*}

$$\varepsilon_{\text{neighbor},i,\text{new}} = \varepsilon_{\text{neighbor},i} + VF_{\text{tr}} \frac{V_{\text{neighbor},i}}{\sum_j \varepsilon_{\text{neighbor},j}} \quad (7)$$

2.2.2 Flow

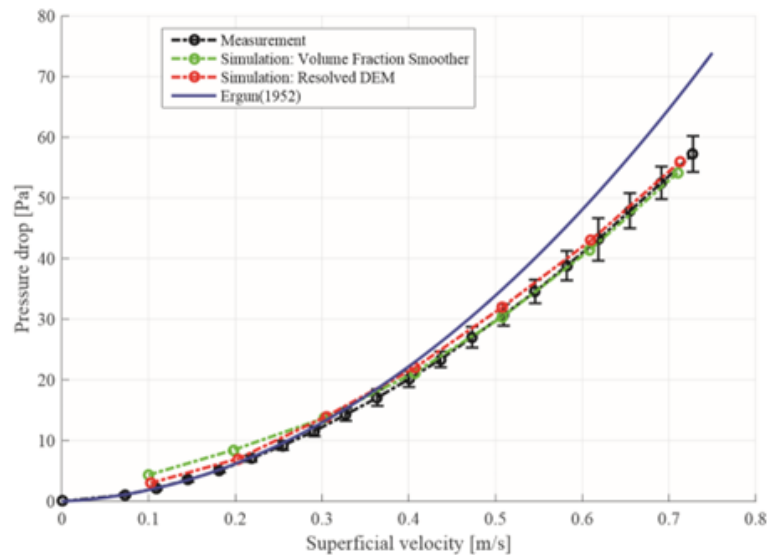
Shaft furnaces are only partially filled with particles. So, the conservation equations must differentiate between the packed bed and the free fluid flow. If the volume fraction in a cell is higher than 0.1, the approach for the packed bed is used. The momentum equation (Eq. (8)) uses different viscosity terms S_μ based on the regime.

$$\frac{\partial}{\partial t}(\rho \varepsilon \underline{u}) + (\underline{u} \nabla)(\rho \varepsilon \underline{u}) + S_\mu = -\nabla(\rho \varepsilon) + \rho \varepsilon g \quad (8)$$

For the free-flow regime, a turbulence-based viscosity pressure drop equation (Eq. (9)) is used. To model the effective viscosity μ_{eff} , the sum of the laminar and the turbulent viscosity is used in the standard k - ε model [12].

$$S_\mu = \mu_{\text{eff}} \nabla^2(\underline{u} \varepsilon) + \frac{1}{3} \mu_{\text{eff}} \nabla(\nabla \underline{u} \varepsilon) \quad (9)$$

Figure 5. Comparison of the pressure drop as a function of the superficial velocity between measurements, the VFS, the resolved DEM, and the Ergun equation in a packed bed of 14-mm glass spheres [1].



In the packed-bed regime, the Ergun equation (Eq. (10)) is used to model the pressure drop.

$$S_\mu = \left[150 \frac{(1-\varepsilon)^2}{\varepsilon^3} \frac{\eta_f U_{s,f,i}}{d_p^2} + 1.75 \frac{1-\varepsilon}{\varepsilon^3} \frac{\rho_f U_{s,f,i} |\bar{U}_{s,f}|}{d_p} \right] \frac{1}{\varepsilon(1-\varepsilon)} \quad (10)$$

To evaluate the implemented model, an experiment was set up, using a 145-mm-high packed bed of 14-mm glass spheres and a 155-mm free-flow region. The pressure drop for different superficial velocities was measured. This bed was modeled using the VFS and a resolved DEM approach. As shown in Fig. 5, both models show good agreement with the experimental data. The Ergun equation deviates at higher superficial velocities, due to wall effects on the volume fraction.

2.2.3 Enthalpy

The equation for the enthalpy (Eq. (11)) is adapted for the gas phase volume fraction ε and has a source term for the heat of combustion S_{comb} calculated from the combustion model, corrected by the gas phase volume fraction and the source for the practice-gas heat transfer S_p . This source term is modeled using a heat exchange model by Gunn [5].

$$\frac{\partial}{\partial t}(\rho \epsilon h) + \nabla(\rho \epsilon u h) - \nabla(\alpha_{\text{eff}} \epsilon \nabla h) = S_p + \epsilon S_{\text{comb}} \quad (11)$$

2.2.4 Species

The species equations (Eq. (12)) have a similar structure as the energy equation (Eq. (11)). The particle source term S_{p,Y_i} describes the emitted or consumed gas from a particle due to drying or chemical reaction. The source term for the combustion S_{comb,Y_i} is calculated by the combustion model and must be corrected by the gas phase volume fraction ϵ .

$$\frac{\partial}{\partial t}(\rho \epsilon Y_i) + \nabla(\rho \epsilon u Y_i) - \nabla(\mu_{\text{eff}} \epsilon \nabla Y_i) = S_{p,Y_i} + \epsilon S_{\text{comb},Y_i} \quad (12)$$

2.2.5 Combustion

To model the chemical reactions of the combustion process, the partially stirred reactor model (PaSR) by Peng Kärholm [13] implemented in OpenFOAM [2] is used. To ensure reasonable computing effort, the four-step global mechanism by Jones and Lindstedt [14] is in use.

2.3 Time Scale Splitting Method

The model of the shaft furnace is transient. In the industrial process, the particles have a residence time of ~ 6 h in the kiln. To reach a quasi-steady-state condition in the furnace, Pollhammer [1] developed the TSSM. The unaccelerated time-step is used for the gas phase equations, and the collision sub-steps, for the granular phase. For the particle fluxes, an accelerated time scale is introduced. The relation between the time scales is called the acceleration factor Γ , and all particle fluxes like mass flow (Eq. (13)), heat (Eq. (14)), and the species (Eq. (15)) of particles flowing into the furnace are multiplied by this predefined factor. Here, $\dot{m}_{p,\text{model}}$ is the mass flow of particles in the model and $\dot{m}_{p,\text{set}}$ is the mass flow specified in the boundary conditions. $S_{p,p,\text{konv}}$ represents the convective heat flux from Eq. (1) and S_p is from Eq. (11). S_{p,p,Y_i} is the source term for the particle species equation and S_{p,Y_i} describes the source term in the enthalpy equation of the gas phase (Eq. (12)).

$$\dot{m}_{p,\text{model}} = \Gamma \dot{m}_{p,\text{set}} \quad (13)$$

$$S_{p,p,\text{konv}} = -\Gamma S_p \quad (14)$$

$$S_{p,p,Y_i} = \Gamma S_{p,Y_i} \quad (15)$$

Due to the time scale splitting, the particle velocity v_p in the shaft furnace increases. This has an impact on the relative velocity and thereby on the heat and mass transfer coefficients. Therefore, a corrected particle velocity $v_{p,\text{corr}}$ was introduced.

$$v_{p,\text{corr}} = \frac{v_p}{\Gamma} \quad (16)$$

To evaluate the TSSM, the heating up of a fixed bed with a height of 150 mm was simulated, with and without time scale splitting. The particles in this bed have a diameter of 10 mm, and a temperature of 300 K as the initial condition. Air with a superficial velocity of 0.5 m s^{-1} and a temperature of 400 K is injected from the bottom of the bed. Fig. 6 compares the particle temperatures at 20, 50, and 100 mm bed height, between the unaccelerated case and by using the TSSM with an acceleration factor of 200. The maximum deviation between the cases is 8 % for the particles at 100 mm. The calculation time using the TSSM with a factor of 200 can be reduced to 2 % in this test case.

3 Shaft Furnace

The presented shaft furnace is used for spinel production, where the crystal structure is changed at 2130 K and no heterogeneous reactions occur. The furnace has a height of 10 m and an inner diameter of 0.85 m. At 3000 kg h^{-1} , particles with a diameter range from 16 to 19.5 mm are fed from the top by a hopper (Fig. 7). The off-gas is extracted with a side pipe under the hopper. At the height of 8 m, 12 premixed air/natural gas burners with a diameter of 15 mm are installed, flush fitting to the wall in a circular arrangement (Fig. 6). The particles are extracted at the bottom of the shaft, and $2000 \text{ Nm}^3 \text{ h}^{-1}$ of secondary air is fed into the furnace.

3.1 Model of the Shaft Furnace

The mesh of the furnace consists of 6.3 million hexahedral cells. The furnace is filled with ~ 1.8 million particles. For the simulation, an acceleration factor of 678 for the TSSM was

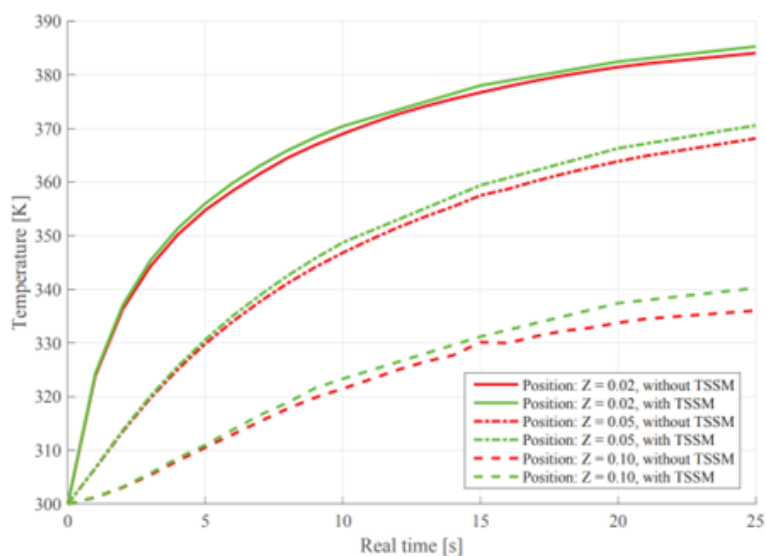


Figure 6. Comparison of the temperatures in a packed bed, with and without using the TSSM [1].

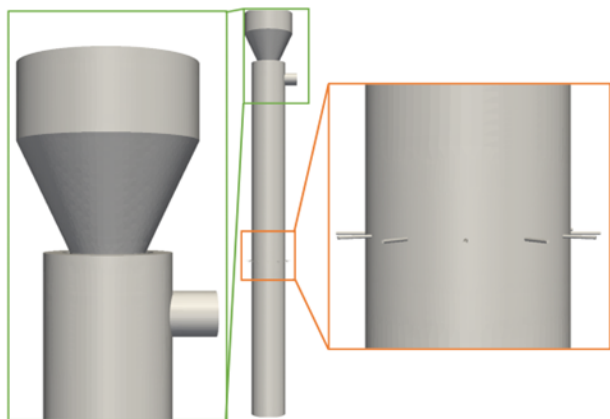


Figure 7. Geometry of the shaft furnace. At the top, the feeding hopper and the exhaust pipe are shown (green). In the middle section, 12 premixed burners are installed (orange).

used. Particles are introduced at 3000 kg h^{-1} at the top part of the hopper (Fig. 8; particle temperature) at 300 K and the according size distribution table, ranging from 16 to 19.5 mm. The same mass flow of particles that are in contact with the bottom surface of the shaft furnace is taken out of the calculation to achieve a consistent filling level. This surface is also a volume flow inlet for $2000 \text{ Nm}^3 \text{ h}^{-1}$ of secondary air at 300 K. At the outlet of the off-gas pipe, the pressure is fixed at 10^5 Pa . The burners are modeled by mass flow inlets with a near stoichiometric natural gas-air mixture. For modeling the thermal boundary conditions of the walls, different thermal transmittance coefficients and a free stream temperature of 320 K are used. To fill the furnace to the initial state, the icoUncoupledKinematicParcelFoam solver from OpenFOAM 2.4.0 [2] was used. The particles were introduced by the inlet until the target filling level was reached. The region where the burners are located was set to 2000 K in the gas phase for ignition.

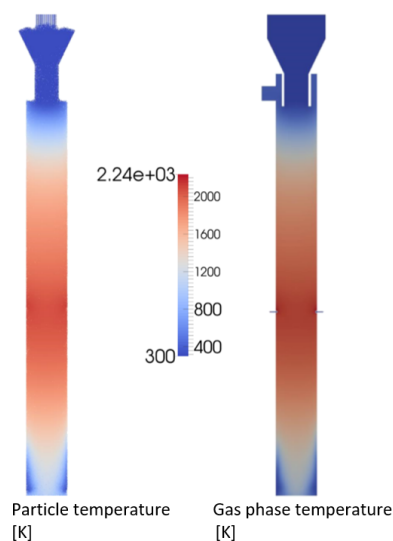


Figure 8. Modeled particle temperature in the furnace (left). Modeled gas phase temperature in the furnace (right).

4 Results

The temperature profiles of the gas and particle phases (Fig. 8) are nearly identical, due to the high heat transfer coefficients ranging from 120 to $300 \text{ W m}^{-2} \text{ K}^{-1}$. The particles reach a maximum temperature of 2243 K at the reaction zone of the burners. In the center of the furnace, at the same height, the temperature reaches 2209 K. These results agree with the operation window of the furnace. The minimum temperature for changing the crystal structure is 2130 K and the maximum temperature is limited by the solidus temperature of the particle at 2320 K. The dominant heat transfer mechanism in the hotter sections of the furnace is particle-particle radiation, leading to a low radial temperature gradient. The radial temperature profiles form in the top and bottom part of the furnace, where the temperatures are lower and particle-particle radiation is less dominant. The particle-particle conduction has no significant impact on the temperature profile, due to the low heat fluxes in comparison to the radiation at the high temperatures in the furnace. The pressure drop between the exhaust duct and the secondary air inlet, at the bottom of the furnace, is predicted at $67 \times 10^3 \text{ Pa}$. The control system of the furnace measures an average pressure drop of $62 \times 10^3 \text{ Pa}$.

5 Summary

Modeling an industrial shaft furnace with a CFD-DEM approach is challenging due to the large number of particles and long process times. The granular phase in the presented spinel shaft furnaces is modeled by 1.8 million particles. To avoid using a resolved DEM approach, the VFS was developed. This approach can predict the pressure drop and fluid flow in the packed bed. This was shown by modeling a laboratory-scale test and the industrial furnace. To avoid the transient modeling of long process times, the TSSM was developed. This method separates the time scales and corrects the fluxes accordingly. This allows reducing the processing time that must be modeled by a factor of up to 680. The method showed an up to 8 % temperature difference for the transient heating up of particles compared to the DEM without TSSM. This difference should decrease when a quasi-steady-state condition is achieved, like in the shaft furnace. The model predicted maximal temperatures inside the operation window of the furnace from 2130 to 2320 K. A weak point of the model presented is the implementation of combustion. The combustion model considered is basically valid for turbulent combustion in an unconfined space. However, in the void spaces among the particles, the heat released by the combustion process is absorbed quickly by the neighboring particles. This effect should be considered in the combustion model and is part of our future work. For the shaft furnace, this assumption does not have a significant impact. The heat of the combustion process is rapidly distributed due to the particle-particle radiation. In the future, an improvement of the combustion model is intended.

The authors have declared no conflict of interest.

Symbols used

A_p	[m ²]	particle surface
$A_{p,p}$	[m ²]	particle-particle contact surface
$A_{p,w}$	[m ²]	particle-wall contact surface
c	[-]	force coefficient
C_p	[-]	static pressure coefficient
c_p	[J kg ⁻¹ K ⁻¹]	heat capacity of the particles
d	[m]	diameter
g	[m s ⁻²]	gravity
h	[J kg ⁻¹]	relative enthalpy
m_p	[kg]	mass of the particle
p	[Pa]	absolute pressure
R_{th}	[m K W ⁻¹]	thermal resistance
t	[s]	time
T	[K]	temperature
S_p	[J m ⁻³ s ⁻¹]	enthalpy particle source term
$S_{p,p,kon}$	[W]	particle-particle conductive heat flux
$S_{p,p,konv}$	[W]	particle-particle convective heat flux
$S_{p,p,rad}$	[W]	particle-particle radiative heat flux
$S_{p,w,kon}$	[W]	particle-wall conductive heat flux
$S_{p,w,konv}$	[W]	particle-wall convective heat flux
$S_{p,w,rad}$	[W]	particle-wall radiative heat flux
S_{p,Y_i}	[kg m ⁻³ s ⁻¹]	particle species source term
S_μ	[kg m ⁻² s ⁻²]	viscosity term
u	[m s ⁻¹]	gas phase velocity
U	[m s ⁻¹]	relative velocity
Y_i	[kg m ⁻² s ⁻¹]	mass fraction of the species i

Greek symbols

α	[W m ⁻¹ K ⁻¹]	thermal conductivity
δ	[-]	Kronecker delta
ε	[-]	gas volume fraction
μ	[Pa s]	gas phase viscosity
ρ	[kg m ⁻³]	gas phase density
σ	[W m ⁻² K ⁻⁴]	Stefan-Boltzmann constant

Sub-/superscripts

cell	cell
comb	combustion
eff	effective, from the turbulence model
p	particle
i, j, m	direction index

Abbreviations

CFD	computational fluid dynamics
DEM	discrete-element method
TSSM	time scale splitting method
VFS	volume fraction smoother

References

- [1] W. R. Pollhammer, A CFD-DEM model for nitrogen oxide prediction in shaft furnaces using OpenFOAM, *Ph.D. Thesis*, Montanuniversitaet Leoben, Leoben **2019**.
- [2] <https://github.com/OpenFOAM/OpenFOAM-2.4.x> (accessed on June, 2014).
- [3] P. A. Cundall, O. D. L. Strack, A discrete numerical model for granular assemblies, *Geotechnique* **1979**, *29*, 47–65.
- [4] D. Höhner, S. Wirtz, V. Scherer, Experimental and numerical investigation on the influence of particle shape and shape approximation on hopper discharge using the discrete element method, *Powder Technol.* **2013**, *235*, 614–627.
- [5] D. J. Gunn, Transfer of heat or mass to particles in fixed and fluidised beds, *Int. J. Heat Mass Transfer* **1978**, *21*, 467–476.
- [6] X. Zhang, P. Cong, S. Fujiwara, M. Fujii, Analysis of heat transfer between two particles for DEM simulations, presented at the *12th International Conference on Fluidization*, Vancouver **2007**.
- [7] K. Kuwagi, M. A. B. Mokhtar, T. Takami, M. Horio, Analysis of heat transfer between two particles for DEM simulations, in *Proc. of the 12th Int. Conf. on Fluidization*, ECI, New York **2007**, 241–248.
- [8] Y. T. Feng, K. Han, An accurate evaluation of geometric view factors for modelling radiative heat transfer in randomly packed beds of equally sized spheres, *Int. J. Heat Mass Transfer* **2012**, *55*, 6374–6383.
- [9] S. Yagi, D. Kunii, Studies on effective thermal conductivities in packed beds, *AIChE J.* **1957**, *3*, 373–381.
- [10] G. T. Nguyen, E. L. Chan, T. Tsuji, T. Tanaka, K. Washino, Resolved CFD-DEM coupling simulation using volume penalisation method, *Adv. Powder Technol.* **2012**, *23*, 225–236.
- [11] H. Xiao, J. Sun, Algorithms in a robust hybrid CFD-DEM solver for particle-laden flows, *Commun. Comput. Phys.* **2011**, *9*, 297–323.
- [12] B. E. Launder, D. B. Spalding, The numerical computation of turbulent flows, *Comput. Methods Appl. Mech. Eng.* **1974**, *3*, 269–289.
- [13] F. Peng Kärholm, Numerical modelling of diesel spray injection, turbulence interaction and combustion, *Ph.D. Thesis*, University Göteborg, Göteborg **2008**.
- [14] W. P. Jones, R. P. Lindstedt, Global reaction schemes for hydrocarbon combustion, *Combust. Flame* **1988**, *73*, 222–233.